Efficiency of Initiating Cell Adhesion in Hydrodynamic Flow

C. Korn[1,2] and U. S. Schwarz[1]

[1]*University of Heidelberg, Im Neuenheimer Feld 293, D-69120 Heidelberg, Germany*
[2]*Max Planck Institute of Colloids and Interfaces, D-14424 Potsdam, Germany*
(Received 19 April 2006; published 28 September 2006)

We theoretically investigate the efficiency of initial binding between a receptor-coated sphere and a ligand-coated wall in linear shear flow. The mean first passage time for binding decreases monotonically with increasing shear rate. Above a saturation threshold of the order of a few 100 receptor patches, the binding efficiency is enhanced only weakly by increasing their number and size, but strongly by increasing their height. This explains why white blood cells in the blood flow adhere through receptor patches localized to the tips of microvilli, and why malaria-infected red blood cells form elevated receptor patches (*knobs*).

Cohesion in biological systems and biotechnological applications is usually provided by specific bonds between receptors and ligands. The formation of these bonds requires a physical transport process which brings receptors and ligands to sufficient proximity for binding. On the cellular level, one of the most prominent examples is the binding of blood-born cells to the vessel walls under the conditions of hydrodynamic flow. For white blood cells, initial binding to the vessel walls is the first step in their hunt for pathogens, which is then followed by rolling adhesion, firm arrest, and extravasation [1]. Similar processes are used by stem and cancer cells which travel the body with the blood stream. Initiating binding to vessel walls is also essential for malaria-infected red blood cells in order to avoid clearance by the spleen and possibly also to foster rupture and release of new parasites into the blood stream [2]. Similar questions about initial binding under flow conditions arise for bacteria, e.g., when binding to the intestinal wall [3], and in biotechnological applications, e.g., for adhesion-based cell sorting [4]. In order to control shear flow and cell density in a quantitative way, standard setups are flow chambers [5]. An essential but largely unexplored aspect of these processes is receptor geometry, that is, size, height, and separation distance of the receptor patches. One way to address this issue experimentally is the use of receptor-coated beads [6].

Earlier theoretical efforts in this context have been focused mainly on issues related to white blood cells, including modeling of the initiation of adhesion at high cell densities (e.g., due to hydrodynamic interactions) [7] and the process of rolling adhesion [8]. In these studies, the parameters characterizing receptor-ligand binding are usually fixed at physiologically motivated values. In this Letter, we take a more general view and ask how a variable receptor geometry affects cell capture in hydrodynamic flow. In order to study this issue in a systematic way, we spatially resolve receptors and ligands. The cell is modeled as a rigid spherical Brownian particle in linear shear flow carrying receptors for ligands covering a planar boundary

wall. In the absence of interactions with other particles or external forces, there is no reason for such a particle to drift towards the wall and initial binding has to rely completely on thermal diffusion. In order to arrive at a generic model, we consider the simplest of the possible downward driving forces in experiments with flow chambers, namely, gravity. The particle is set free at a certain height above the wall and we calculate the mean first passage time (MFPT) for the first receptor-ligand encounter as a measure for the efficiency of initial cell binding. We consider three models of increasing complexity in regard to the spatial distribution of receptors and ligands. We first show that if the receptors on the cell and the ligands on the substrate are distributed homogeneously, then the corresponding MFPTs can be calculated exactly. In the case that receptors are spatially resolved, we use extensive computer simulations to calculate the MFPTs as a function of their number and spatial dimensions, both in two and three dimensions. As a third case, we in addition consider spatially resolved ligand distribution.

Figure 1 introduces the parameters of our model. We consider a sphere of radius R which moves with the hydrodynamic flow in positive x direction at a height z above the wall with normal $\mathbf{e}_z$. The simplest possible flow pattern is linear shear flow with shear rate $\dot{\gamma}$. With the no-slip boundary condition at the wall, the unperturbed velocity profile reads $\mathbf{u}^\infty = \dot{\gamma} z \mathbf{e}_x$. For a typical cell radius $R = 5$ μm and a typical shear rate $\dot{\gamma} = 100$ Hz, the Reynolds number in aqueous solution is well below 1 and the hydrodynamic flow is essentially described by the Stokes equation for incompressible fluids. This is even more true for smaller particles like micron-sized beads. Scaling estimates also show that for typical parameter values for cell elasticity, deformations due to shear flow and lubrication forces are small and therefore the spherical approximation is justified. In addition to the hydrodynamic forces, in our model there are also gravitational and thermal forces acting on the particle. Such a combination of forces is the subject of Stokesian dynamics [9] and in our case leads to the follow-
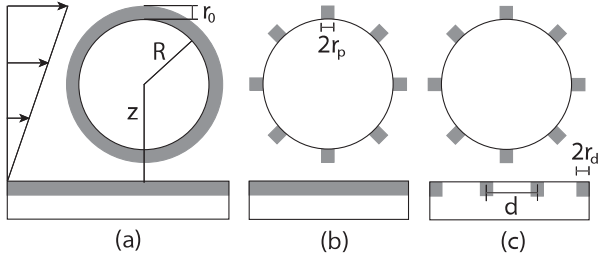
FIG. 1.   A cell of radius R moves in linear shear flow above a wall at a height z, subject to hydrodynamic, gravitational, and thermal forces. The efficiency for initiating binding is assessed by calculating the mean first passage time for approach of receptor and ligand to a capture distance r_0, that is, for overlap of the gray regions. Three models of increasing complexity are studied here: (a) homogeneous coverage of cell and wall, (b) N_r equidistantly placed receptor patches on the cell, each with radius r_p, and (c) ligand patches of radius r_d separated by distance d.

ing Langevin equation [10]:

$$\partial_t \mathbf{X}_t = \mathbf{u}^\infty + \mathsf{M}(\mathbf{F}^G + \mathbf{F}^S) + k_B T_a \mathsf{B} \nabla \mathsf{B}^T + \mathbf{g}_t^S. \quad (1)$$

T_a is ambient temperature. The gravitational force reads $\mathbf{F}^G = -g\Delta\rho(4\pi R^3/3)\mathbf{e}_z$ with some density difference $\Delta\rho$. The subscript t denotes random variables. As usual, the thermal force $\mathbf{g}_t$ is assumed to be Gaussian:

$$\langle \mathbf{g}_t \rangle = 0, \qquad \langle \mathbf{g}_t \mathbf{g}_{t'} \rangle = 2k_B T_a \mathsf{M} \delta(t - t'). \quad (2)$$

The superscript S for the multiplicative noise term in Eq. (1) indicates that it has to be interpreted in the usual Stratonovich sense. The matrix B in Eq. (1) is related to the mobility matrix M through $\mathsf{M} = \mathsf{B}\mathsf{B}^T$. Vectors in Eq. (1) are six dimensional, representing the spatial and orientational degrees of freedom. The mobility matrix M and the shear force $\mathbf{F}^S$ for a spherical particle above a wall cannot be obtained in analytically closed form. However, they can be calculated numerically to high accuracy and we will use this for our simulations [11].

Considering the physical dimensions of our problem shows that the motion of the cell is essentially governed by two dimensionless numbers. For length, the natural scale is cell radius R. Mobility and shear force scale as $M = 1/(6\pi\eta R)$ and $F^S = 6\pi\eta R^2 \dot\gamma$, respectively. For time, there are two relevant time scales, the deterministic time scale $1/\dot\gamma$ and the diffusive time scale $R^2/D = 6\pi\eta R^3/k_B T_a$, where we have used the Einstein relation $D = M k_B T_a$ for the diffusion constant D. Therefore, the relative importance of hydrodynamic to thermal motion is described by the Péclet number $\mathrm{Pe} = 6\pi\eta R^3 \dot\gamma/k_B T_a$. In the limits $\mathrm{Pe} \to 0$ and $\mathrm{Pe} \to \infty$, diffusive and deterministic motion dominate, respectively. The gravitational force introduces another dimensionless number, which we call the Péclet number in z direction, $\mathrm{Pe}_z = F^G R/k_B T_a = 4\pi g\Delta\rho R^4/(3k_B T_a)$. In the following, we will nondimen-

sionalize length and time by R and $6\pi\eta R^3/k_B T_a$, respectively.

We start by considering homogeneous coverage of cell and wall with receptors and ligands, respectively, compare Fig. 1(a). Then rotational degrees of freedom are irrelevant. Because the wall breaks the symmetry only in the z direction, motion in the x-y plane is decoupled from our problem. Thus in this case we essentially deal with a MFPT in one dimension, which is independent of shear rate $\dot\gamma$ and which can be approached with standard methods for the appropriate Fokker-Planck equation. Binding is identified with approach of receptor and ligand to a capture distance r_0. Applied to the case of homogeneous coverage, the cell has to fall to the capture height $1 + r_0$. If dropped from the initial height z_0, the respective MFPT can be shown to be

$$T_h = \frac{1}{\mathrm{Pe}_z} \int_{1+r_0}^{z_0} dz \frac{1}{M_{zz}(z)}. \quad (3)$$

Thus the MFPT scales inversely with the gravitational force driving the cell onto the wall. With the lubrication approximation $M_{zz}(z) \approx 1 - 1/z$ we find

$$T_h \approx \frac{1}{\mathrm{Pe}_z}\left[z_0 - 1 - r_0 + \ln\left(\frac{z_0 - 1}{r_0}\right)\right]. \quad (4)$$

Thus the MFPT diverges logarithmically with vanishing capture distance r_0 (that is, when the cell has to get infinitely close to the wall) and linearly with initial height z_0 (that is, when the cell starts infinitely far away from the wall). Although only the constant force chosen here results in an analytical result like Eq. (4), for other types of force laws it is straightforward to numerically calculate corresponding falling times T_h [10].

We next consider the case of a spatially resolved receptor distribution, compare Fig. 1(b). Now the cell is equidistantly covered with N_r receptor patches, each with radius r_p and height r_0. We first note that in this case, initial orientation becomes important. Moreover, now shear rate $\dot\gamma$ enters the analysis: the shear flow increases cell rotation, and for heterogeneous receptor coverage, this strongly influences when the first receptor can bind the first ligand. Because experimentally it is hardly possible to prepare the initial orientation of the cell, in the following we average over all possible initial orientations. One can show that the angle-averaged MFPT is the MFPT to fall from initial height z_0 to some intermediate height z_m according to Eq. (3) (that is independent of orientation) plus the angle-averaged MFPT to bind from the initial height z_m. In this sense, the initial height is not relevant for our problem and in the following we always use $z_0 = 2$, that is the cell has to fall for the distance of one radius before binding can occur.

In Figs. 2(a) and 2(b) we show the MFPT as obtained by extensive computer simulations as a function of Péclet number $\mathrm{Pe} \sim \dot\gamma$ and receptor patch number N_r for two (2D) and three dimensions (3D), respectively. Here 2D
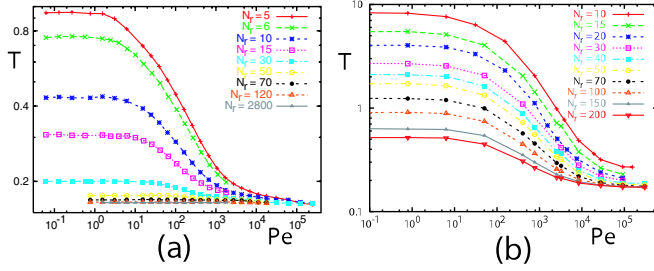
FIG. 2 (color online).   Effect of shear rate on mean first passage time T for initial binding for spatially resolved receptors in (a) two (2D) and (b) three dimensions (3D). The scales for length and time are R and $6\pi\eta R^3/k_B T_a$, respectively. The Péclet number $\mathrm{Pe} = 6\pi\eta R^3\dot{\gamma}/k_B T_a$ and the Péclet number in z direction $\mathrm{Pe}_z = 4\pi g\Delta\rho R^4/(3k_B T_a)$ represent the strengths of the hydrodynamic and gravitational forces, respectively, relative to the thermal forces. $z_0 = 2$, $\mathrm{Pe}_z = 50$, $r_0 = r_p = 10^{-3}$.

means that translational motion is restricted to the x-z plane and rotations are restricted about the y axis, which allows for much faster simulations. Each data point in Fig. 2 is the average of at least 10^5 simulated trajectories of the Langevin equation [Eq. (1)]. Our simulations are very time consuming because with the receptor patches we resolve objects of typical size 10^{-3}, that is, nm-sized patches on micron-sized cells. From Fig. 2 we first note that T decreases monotonously with increasing Pe and that the shear rate does not change the relative sequence of the curves for different N_r. Thus the larger shear rate and the more receptor patches present, the more efficient cell capture. The crossover between the diffusion- and convection-dominated regimes does not occur at $\mathrm{Pe} \approx 1$, but at much larger values $\mathrm{Pe} \approx 10^2$. Next we note that in the 2D case [Fig. 2(a)], for large Pe or large N_r, all curves level off to the exact result for homogeneous coverage from Eq. (3), because in these two limits, the binding process effectively becomes rotationally invariant. In the 3D case [Fig. 2(b)], the homogeneous reference value is only achieved for large receptor numbers. The reason is that for small numbers of receptors, the cell might have to rotate around the x axis before a receptor moving on a circle parallel to the x-z plane is able to bind a ligand on the wall. Therefore, in 3D thermal diffusion remains essential even in the case of large Péclet number.

In order to achieve a better understanding of the simulation results shown in Fig. 2, it is instructive to decompose the process into periods of falling and rotation, respectively. A detailed analysis shows that in the 2D case this decomposition allows to derive scaling laws for different limits in regard to Pe and Pe_z. An important case is the one of large Pe_z, when the cell is strongly driven onto the wall. Then the binding process can be decomposed into a initial falling period described by Eq. (3), followed by a purely rotational search for ligand, which is independent of Pe_z and can be calculated analytically:

$$T_r = \frac{A_\theta\Delta\theta^2 \coth(\frac{A_\theta\Delta\theta}{2D_\theta}) - 2D_\theta\Delta\theta}{2A_\theta^2\theta_s}. \quad (5)$$

Here $\Delta\theta \approx \theta_s$ is the angle between the absorbing boundaries, $\theta_s = 2\pi/N_r$ the angle between receptor patches, $A_\theta \approx \mathrm{Pe}/2$ the rotational drift, and $D_\theta \approx 3/4$ the rotational diffusion constant. From Eq. (5) we get $T \sim 1/N_r^2$ and $T \sim 1/(N_r\mathrm{Pe})$ for small and large Pe, respectively, in excellent agreement with the scaling found in our simulations. In general, Eq. (5) is a good qualitative description of the 2D data shown in Fig. 2.

In order to consider the case of spatially resolved ligand, compare Fig. 1(c), we cover the boundary wall with a square lattice of circular ligand patches, with lattice constant d and patch radius r_d. Because again the Péclet number does not change the relative sequence of the different MFPT curves, the efficiency of initial cell binding as a function of receptor and ligand geometry can be investigated in the diffusive limit $\mathrm{Pe} \approx 0$. Figure 3 shows for this case that the MFPT saturates both when increasing receptor coverage by increasing N_r or ligand coverage by decreasing d. A similar saturation behavior is also found when increasing receptor and ligand patch sizes r_p and r_d. Typically the saturation threshold for the parameters used is located at a mean patch-to-patch distance d of about 0.17, both in regard with receptors and ligands. For a coverage below the threshold, Fig. 3 shows that the MFPT scales like $\sim 1/N_r \sim d^2$ and $\sim 1/\rho_l \sim d^2$ in regard to receptor and ligand coverage, respectively, where d represents the distance between receptor and ligand patches, respectively. This can be understood by noting that the 1D MFPT for capture by diffusion scales $\sim d^2$ where d is the distance between the two absorbing boundaries. The saturation effect observed with respect to N_r, ρ_l, r_p, and r_d results from the space-filling nature of diffusion which has been implicated before for the efficiency of ligand capture by a cell [12].
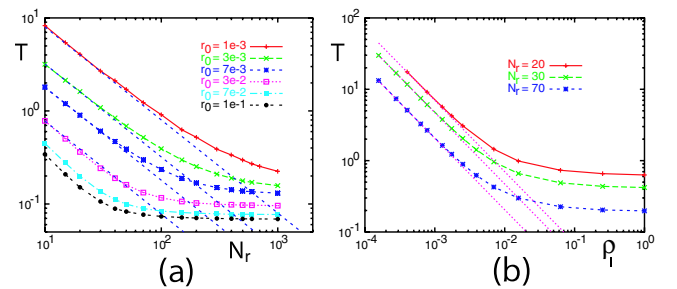

FIG. 3 (color online).   Mean first passage time T in 3D in the diffusive limit ($\mathrm{Pe} \approx 0$) as a function of (a) the number of receptor patches N_r for different values of patch height r_0 and (b) ligand density ρ_l as varied by decreasing ligand patch distance d for different values of the number of receptors N_r. The dashed lines show the scaling behaviors $T \sim 1/N_r$ and $T \sim 1/\rho_l$ at low receptor and ligand coverage, respectively. $z_0 = 2$, $\mathrm{Pe}_z = 50$, $r_0 = r_p = r_d = 10^{-2}$.
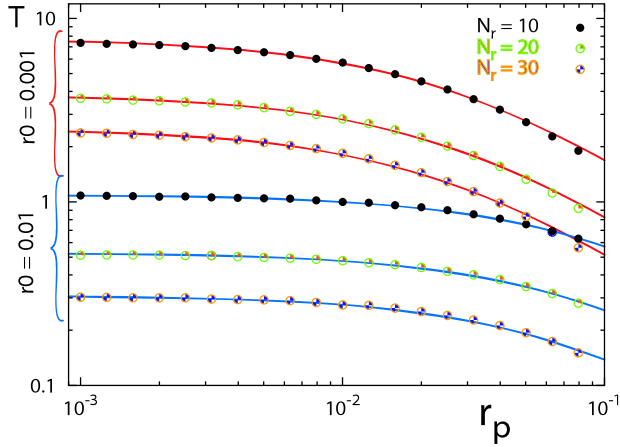
FIG. 4 (color online).   Mean first passage time T in 3D in the diffusive limit (Pe ≈ 0) as a function of the receptor patch radius r_p for two different values of r_0 and three different values of N_r. For better comparison with regard to r_0 the mean first passage time T_h for homogeneous coverage from Eq. (3) has been subtracted. The lines are fits according to Eq. (6). Other parameters as in Fig. 2.

We finally turn to the effect of the capture distance r_0. In Fig. 4 we show the MFPT in the diffusive limit as a function of the receptor patch radius r_p for $r_0 = 10^{-3}$ and $r_0 = 10^{-2}$ as well as for three different values of N_r. We first note that the MFPT is much more influenced by a change in r_0 or N_r than by a change in r_p. One can show on geometrical grounds that the two parameters r_0 and r_p conspire to define an effective receptor patch size $\sqrt{r_0} + r_p$ which then in turn determines the probability for binding. This line of reasoning leads to the formula

$$T = \frac{a}{b + r_p} + T_h, \qquad (6)$$

where $a = 2t_d/\sqrt{r_0}$, $b = \sqrt{r_0}/2$, t_d is a typical diffusion time between binding attempts which scales $\sim 1/N_r$, and T_h is the homogeneous result from Eq. (3). Equation (6) implies that even for vanishing receptor size the MFPT remains finite due to a finite r_0. The lines in Fig. 4 show that this equation can be fitted extremely well to the simulation results. Moreover, the fitted values for a and b agree roughly with the predicted scaling behavior.

In summary, our results show that the efficiency for initiating cell adhesion in hydrodynamic flow is strongly enhanced by increasing the number of receptor patches N_r, but only up to a saturation threshold. An increase of patch size r_p leads only to a weak enhancement of binding efficiency. In contrast, a strong enhancement results from increasing the patch height r_0. For example, for a few hundred receptor patches, an elevation of $r_0 = 10^{-2}$ makes initial binding already as efficient as for a homogeneously covered cell. Strikingly, white blood cells are indeed characterized by such a receptor geometry, because they are covered with hundreds of protrusions (*microvilli*, typical height 300 nm, corresponding to $r_0 = 0.06$) which carry adhesion receptors like *L*-selectin at their narrow tips [5]. In general, white blood cells operate in the limit of a homogeneously covered cell not only due to their receptor geometry, but also because during capture they are usually exposed to environments with Pe ≈ 10^4–10^5 (a typical value for Pe$_z$ is 300). The principle of enhancing capture efficiency by elevation of receptor patches seems to be also used by other biological systems. One example of large medical relevance appears to be malaria-infected red blood cells, which develop thousands of little adhesive protrusions (*knobs*, typical height 20 nm, corresponding to $r_0 = 0.004$) [2]. The results presented here do not only allow to understand the efficiency of cell capture in these biological systems in a unified way, but can also be used for developing corresponding applications in biotechnology, including adhesion-based cell or particle sorting.

[1] T. A. Springer, Cell **76**, 301 (1994).
[2] E. Nagao, O. Kaneko, and J. A. Dvorak, J. Struct. Biol. **130**, 34 (2000); L. Bannister and G. Mitchell, Trends Parasitol. **19**, 209 (2003).
[3] W. Thomas, E. Trintchina, M. Forero, V. Vogel, and E. Sokurenko, Cell **109**, 913 (2002).
[4] M. Forero, W. Thomas, C. Bland, L. Nilsson, E. Sokurenko, and V. Vogel, Nano Lett. **4**, 1593 (2004).
[5] R. Alon, D. A. Hammer, and T. A. Springer, Nature (London) **374**, 539 (1995); S. Chen and T. A. Springer, Proc. Natl. Acad. Sci. U.S.A. **98**, 950 (2001); O. Dwir, A. Solomon, S. Mangan, G. S. Kansas, U. S. Schwarz, and R. Alon, J. Cell Biol. **163**, 649 (2003).
[6] A. Pierres, D. Touchard, A.-M. Benoliel, and P. Bongrand, Biophys. J. **82**, 3214 (2002).
[7] M. R. King and D. A. Hammer, Proc. Natl. Acad. Sci. U.S.A. **98**, 14 919 (2001); C. Sun, C. Migliorini, and L. L. Munn, Biophys. J. **85**, 208 (2003).
[8] K.-C. Chang, D. F. J. Tees, and D. A. Hammer, Proc. Natl. Acad. Sci. U.S.A. **97**, 11 262 (2000).
[9] D. L. Ermak and J. A. McCammon, J. Chem. Phys. **69**, 1352 (1978); J. F. Brady and G. Bossis, Annu. Rev. Fluid Mech. **20**, 111 (1988).
[10] A detailed derivation of the Langevin equation and more details of our simulation algorithms and results will be published elsewhere.
[11] G. S. Perkins and R. B. Jones, Physica (Amsterdam) **A189**, 447 (1992); B. Cichocki and R. B. Jones, Physica (Amsterdam) **A258**, 273 (1998).
[12] H. C. Berg and E. M. Purcell, Biophys. J. **20**, 193 (1977); D. Shoup and A. Szabo, Biophys. J. **40**, 33 (1982).